JOURNAL OF GUIDANCE, CONTROL, AND DYNAMICS
Vol. 39, No. 6, June 2016

Engineering Notes

Passivity-Based Adaptive Control of Robotic Spacecraft for Proximity Operations Under Uncertainties

Steve Ulrich*
Carleton University, Ottawa, Ontario K1S 5B6, Canada
Alvar Saenz-Otero†
Massachusetts Institute of Technology, Cambridge, Massachusetts 02139
and
Itzhak Barkana‡
Barkana Consulting, 47209 Ramat-Hasharon, Israel

DOI: 10.2514/1.G001491

I. Introduction

THE Defense Advanced Research Projects Agency (DARPA) initiated the Phoenix Program, a venture to build on the success of the Japan Aerospace Exploration Agency's Engineering Test Satellite VII [1] and Boeing's Orbital Express [2] proximity operation demonstration missions. One of the objectives of this program is to develop and demonstrate a new class of small modular satlets, similar to nanosatellites, capable of assisting in the retrieval of valuable components from depleted satellites in geosynchronous orbits for use in the assembly of new space systems.§ As part of the first demonstration mission under this program, the free-flyer robots will be required to manipulate a variety of components of different mass, such as space apertures and antennas. In this context, the relative position control systems must be robust to uncertainties in the free-flyer robot mass to ensure consistent and safe relative motion control with minimal trajectory overshoots.

In close-proximity operations, the spacecraft would typically be close enough to employ the Clohessy–Wiltshire equations [3] to model the relative dynamics. Furthermore, when the time scale is significantly less than the orbital period of the target spacecraft, and the distance between both vehicles is limited to a few meters, a simple double-integrator model can be applied [4]. Being linear, these dynamics representations are particularly attractive for control purposes, which is why the literature proposes numerous linear continuous control laws to regulate or track a prescribed relative trajectory. However, most existing continuous control techniques for proximity operations are model-based and can only achieve good tracking performance when substantial information of the plant mathematical model and its dynamics parameters is available (e.g., mass and inertia). If the dynamics parameters are uncertain or there are unmodeled dynamics effects acting on the plant, model-based control approaches could perform inadequately. Dynamics uncertainties may arise when neglecting nonlinear dynamics effects or external perturbations in the plant model, whereas parameter uncertainties may arise from mass-inertia properties that vary due to fuel consumption, solar array deployment, payload variation, or, in the case of DARPA's Phoenix, when the free-flyer servicer robot harvests a component of unknown mass from the target spacecraft.

One way to manage both dynamics and parameter uncertainties is to employ indirect adaptive control techniques, which can, in real-time, identify the unknown plant parameters and external perturbations from which the control gains are obtained using an automatic design procedure. However, this class of adaptive control methodologies requires accurate information about the plant dynamics model [5]. For example, de Queiroz et al. [6] proposed an indirect adaptive control strategy, in which an adaptation law based on precise knowledge of the dynamics model identifies the unknown mass, which is then used explicitly in their control law. An adverse consequence of such identification procedures is the increased computational burden associated with real-time estimation of unknown parameters and dynamics effects. This could rule out using such indirect adaptive controllers for small space robot applications with limited computational resources.

Alternatively, direct adaptive control techniques, with controller gains updated directly without requiring estimates of unknown plant parameters or mathematical models of the system to be controlled, can be used to address this problem. Based on our knowledge, no previous work investigated the use of direct adaptive control techniques for this application. In view of the preceding, this Note addresses the problem of continuous relative motion control under large uncertainties in the plant parameter, dynamics uncertainties, and unmodeled external perturbations, through the development of an output feedback direct adaptive control law.

More specifically, this Note proposes a passivity-based adaptive control strategy derived upon the simple adaptive control (SAC) theory [7]. The stability of the passivity-based adaptive system is guaranteed through the Lyapunov direct method [8] and LaSalle's invariance principle for nonautonomous systems [7,9–11] arguments, by applying the almost strictly passive conditions. These conditions are herein demonstrated to be satisfied by modeling both the Clohessy–Wiltshire and the double-integrator relative dynamics models as square linear time-invariant systems with a scaled-position-to-velocity output matrix. In addition, based on recent development in the area of nonlinear stability [12], this Note clarifies the use of LaSalle's invariance principle (as opposed to the widely used Barbalat's lemma [8]) for this particular problem, where the Lyapunov derivative function is negative-semidefinite. These two aspects correspond to the original theoretical contributions of this work.

Finally, most previous work in the area of close-proximity operations only assessed the performance of the controllers in numerical simulations. In this context, another original contribution of this Note is to validate the passivity-based adaptive controller against a nonadaptive proportional-derivative (PD) controller, through experiments at the Massachusetts Institute of Technology's Synchronized Position Hold Engage Reorient Experimental Satellites (SPHERES) research facility. The experimental results demonstrate that the adaptive control law is applicable for real-time implementation onboard a small free-flyer robot with practical

Presented as Paper 2014-1288 at the AIAA Guidance, Navigation and Control Conference, National Harbor, MD, 13–17 January 2014; received 22 May 2015; revision received 24 December 2015; accepted for publication 4 January 2016; published online 29 March 2016.

*Assistant Professor, Department of Mechanical and Aerospace Engineering, 1125 Colonel By Drive. Senior Member AIAA.
†Research Scientist, Department of Aeronautics and Astronautics, 77 Massachusetts Avenue. Senior Member AIAA.
‡President, 11 Hashomer Street. Associate Fellow AIAA.
§Data available online at http://www.darpa.mil/program/phoenix [retrieved 9 February 2016].

limitations, including limited computing power, mass uncertainty, unknown external perturbations, sensor noise, and nonideal actuators.

II. Almost Strictly Passive Linearized Dynamics

Under the assumption that both the relative position and velocity can be measured, the output of the plant $\boldsymbol{y} \in \mathbb{R}^3$ can be defined as a linear combination of position and velocity:

$$\boldsymbol{y} = [\alpha x + \dot{x} \quad \alpha y + \dot{y} \quad \alpha z + \dot{z}]^T \tag{1}$$

where $[x \quad y \quad z]^T \in \mathbb{R}^3$ and $[\dot{x} \quad \dot{y} \quad \dot{z}]^T \in \mathbb{R}^3$ are the relative position and velocity expressed in the local-vertical–local-horizontal reference frame, which is defined with its x axis aligned with the radial vector of the target spacecraft orbit, its z axis aligned with the orbit angular momentum vector of the target orbit, and its y axis completing the right-handed orthogonal frame. As shown in Eq. (1), $\alpha \in \mathbb{R}$ denotes the positive-definite ratio of position to velocity, such that the relative position can be controlled through the position feedback, whereas the velocity provides beneficial damping effects. Practically, both the relative position and velocity are needed separately to then generate the output through the α term, which is simply a parameter chosen by the user to give weight to the position measurement relative to the velocity measurement. However, the position and velocity are not required separately by the controller. Such an output signal is similar to what is sometimes referred to as a filtered error [13].

More importantly, defining the output as a combined position plus velocity, the states as $\boldsymbol{x} = [x \quad y \quad z \quad \dot{x} \quad \dot{y} \quad \dot{z}]^T \in \mathbb{R}^6$, and the control input forces as $\boldsymbol{u} = [f_x \quad f_y \quad f_z]^T \in \mathbb{R}^3$ allows the linearized relative dynamics applicable to close-proximity operations to be herein described as a square state-space system of the form

$$\dot{\boldsymbol{x}} = \boldsymbol{A}\boldsymbol{x} + \boldsymbol{B}\boldsymbol{u}, \qquad \boldsymbol{y} = \boldsymbol{C}\boldsymbol{x} \tag{2}$$

As it will be shown in this section, modeling the dynamics as a square state-space system is required to determine the positive-definitiveness of the output–input matricial product $\boldsymbol{CB}$.

A. Clohessy–Wiltshire Model

If the target spacecraft orbit is assumed to be circular (or near-circular) and the distance between the two vehicles is relatively small compared to their orbital radii, the nonlinear equations of relative motion simplify to the well-known Clohessy–Wiltshire (CW) equations [3]:

$$\ddot{x} - 3n^2 x - 2n\dot{y} = a_x \tag{3}$$

$$\ddot{y} + 2n\dot{x} = a_y \tag{4}$$

$$\ddot{z} + n^2 z = a_z \tag{5}$$

where $n \in \mathbb{R}$ denotes the orbital mean motion, and $a_j = f_j/m$, $\forall\, j = \{x, y, z\}$, with $m \in \mathbb{R}$ denoting the mass of the free-flyer space robot, such that the appropriately-dimensioned real matrices are given by

$$\boldsymbol{A} = \begin{bmatrix} & \boldsymbol{0}_{3\times3} & & & \boldsymbol{I}_{3\times3} & \\ 3n^2 & 0 & 0 & 0 & 2n & 0 \\ 0 & 0 & 0 & -2n & 0 & 0 \\ 0 & 0 & -n^2 & 0 & 0 & 0 \end{bmatrix},$$

$$\boldsymbol{B} = \begin{bmatrix} \boldsymbol{0}_{3\times3} \\ \frac{1}{m}\boldsymbol{I}_{3\times3} \end{bmatrix}, \qquad \boldsymbol{C} = [\alpha \boldsymbol{I}_{3\times3} \quad \boldsymbol{I}_{3\times3}] \tag{6}$$

B. Double-Integrator Model

As shown in Eqs. (3–5), the in-plane (x-y) and out-of-plane (z) motions are decoupled, with the in-plane coupling terms corresponding to Coriolis and gravity forces, whereas the out-of-plane is an undamped oscillation with the orbital mean motion. As noted by Fehse [4], these terms can be considered low-frequency perturbations to be compensated by a feedback controller, which means that a double-integrator model that is independent for each axis can be used. Also, it can easily be shown that, in close proximity, that is, when the maximum distance is on the order of a few tens of meters, these coupling terms are at least one order of magnitude smaller than the remaining double-integrator terms in the CW equations [14]. This simplification is also justified whenever the spacecraft are maneuvering on a faster time scale than the orbital mean motion n. As explained by Paluszek and Thomas [15], this is evident because the Bode plots of the double-integrator superimposed on the CW equations are identical in frequencies higher than n. With the double-integrator simplification, the input and output matrices in Eq. (6), $\boldsymbol{B}$ and $\boldsymbol{C}$, respectively, remain the same, whereas the system matrix $\boldsymbol{A}$ becomes independent of the orbital mean motion, that is

$$\boldsymbol{A} = \begin{bmatrix} \boldsymbol{0}_{3\times3} & \boldsymbol{I}_{3\times3} \\ \boldsymbol{0}_{3\times3} & \boldsymbol{0}_{3\times3} \end{bmatrix}, \qquad \boldsymbol{B} = \begin{bmatrix} \boldsymbol{0}_{3\times3} \\ \frac{1}{m}\boldsymbol{I}_{3\times3} \end{bmatrix}, \qquad \boldsymbol{C} = [\alpha \boldsymbol{I}_{3\times3} \quad \boldsymbol{I}_{3\times3}] \tag{7}$$

C. Almost Strict Passiveness

Theorem 1: The relative motion models described by the linear time-invariant (LTI) state-space system in Eq. (2), with either the Clohessy–Wiltshire dynamics in Eq. (6) or the double-integrator dynamics in Eq. (7), with scaled-position-and-velocity output matrix are almost strictly passive (ASP), and their transfer functions $\boldsymbol{G}(s) = \boldsymbol{C}(s\boldsymbol{I}_{6\times6} - \boldsymbol{A})^{-1}\boldsymbol{B}$ are almost strictly positive real (ASPR).

Proof: The LTI systems described by Eq. (2) with matrices in either Eq. (6) or Eq. (7) are strictly minimum-phase and have a positive-definite symmetric (PDS) matricial product $\boldsymbol{CB} \in \mathbb{R}^{3\times3}$:

$$\boldsymbol{CB} = [\alpha \boldsymbol{I}_{3\times3} \quad \boldsymbol{I}_{3\times3}] \begin{bmatrix} 0_{3\times3} \\ \frac{1}{m}\boldsymbol{I}_{3\times3} \end{bmatrix} = \frac{1}{m}\boldsymbol{I}_{3\times3} > 0_{3\times3} \tag{8}$$

Both LTI systems are therefore ASP, and their transfer functions are ASPR [16]. As a result, their respective closed-loop system matrix $\boldsymbol{A}_c \in \mathbb{R}^{6\times6}$

$$\boldsymbol{A}_c = \boldsymbol{A} - \boldsymbol{B}\tilde{\boldsymbol{K}}_e\boldsymbol{C} \tag{9}$$

satisfies the Kalman–Yakubovich–Popov conditions

$$\boldsymbol{P}\boldsymbol{A}_c + \boldsymbol{A}_c^T\boldsymbol{P} = -\boldsymbol{Q} \tag{10}$$

$$\boldsymbol{P}\boldsymbol{B} = \boldsymbol{C}^T \tag{11}$$

where $\tilde{\boldsymbol{K}}_e \in \mathbb{R}^{3\times3}$ is a constant fictitious output feedback gain matrix, which is unknown and not needed for implementation, and $\boldsymbol{P}$ and $\boldsymbol{Q}$ are PDS matrices. □

III. Controller Formulation

This section presents the ideal model, defines the control objectives, and provides the details on the control law and its related control gain adaptation mechanisms.

A. Ideal Model

The control objective consists of forcing the outputs of the uncertain closed-loop dynamics to asymptotically track the outputs of the ideal model designed with the prescribed linear form

$$\dot{\boldsymbol{x}}_m = \boldsymbol{A}_m\boldsymbol{x}_m + \boldsymbol{B}_m\boldsymbol{u}_m, \qquad \boldsymbol{y}_m = \boldsymbol{C}_m\boldsymbol{x}_m \tag{12}$$

with the state vector of the ideal model defined as

$$\boldsymbol{x}_m = [\,x_m \quad y_m \quad z_m \quad \dot{x}_m \quad \dot{y}_m \quad \dot{z}_m\,]^T \in \mathbb{R}^6 \tag{13}$$

and the input vector as

$$\boldsymbol{u}_m = [\,x_d \quad y_d \quad z_d\,]^T \in \mathbb{R}^3 \tag{14}$$

where $x_d,\ y_d,\ z_d \in \mathbb{R}$ denotes the desired relative trajectory, and $\boldsymbol{y}_m \in \mathbb{R}^3$ is the model output. Specifically, the desired input–output relative motion response is expressed in terms of the ideal damping ratio $\zeta \in \mathbb{R}$ and the undamped natural frequency $\omega_n \in \mathbb{R}$, as follows:

$$\begin{aligned}
\boldsymbol{A}_m &= \begin{bmatrix} \boldsymbol{0}_{3\times3} & \boldsymbol{I}_{3\times3} \\ -\omega_n^2\boldsymbol{I}_{3\times3} & -2\zeta\omega_n\boldsymbol{I}_{3\times3} \end{bmatrix} \in \mathbb{R}^{6\times6}, \\
\boldsymbol{B}_m &= \begin{bmatrix} \boldsymbol{0}_{3\times3} \\ \omega_n^2\boldsymbol{I}_{3\times3} \end{bmatrix} \in \mathbb{R}^{6\times3}, \\
\boldsymbol{C}_m &= [\,\alpha_m\boldsymbol{I}_{3\times3} \quad \boldsymbol{I}_{3\times3}\,] \in \mathbb{R}^{3\times6}
\end{aligned} \tag{15}$$

This ideal model only represents the desired, or ideal, input–output closed-loop behavior of the relative motion and is not based on any explicit a priori knowledge about the dynamics parameters. Indeed, the preceding differential equation does not contain any system properties.

B. Control Objective

The control objective is to be met under the constraint of no knowledge of the servicer robot mass m and external perturbations. In other words, the uncertainties considered in this study are in the input matrix $\boldsymbol{B}$ and control input matrix $\boldsymbol{u}$. To quantify the control objective, an output tracking error denoted by $\boldsymbol{e}_y \in \mathbb{R}^3$ is defined as

$$\boldsymbol{e}_y \triangleq \boldsymbol{y}_m - \boldsymbol{y} \tag{16}$$

C. Control Law and Adaptation Mechanisms

Because of the uncertainties, the controller will apply a direct adaptation law that varies the control gains in real time in response to the tracking error $\boldsymbol{e}_y$, without generating dynamic parameter estimates. In addition to the output tracking-error signal, the adaptive control methodology, which is based on the command generator tracker methodology [17], uses all available data about the ideal model by including the model states and inputs in a feedforward configuration to compute the control input force accordingly to the SAC theory [7]:

$$\boldsymbol{u}(t) = \boldsymbol{K}_e(t)\boldsymbol{e}_y(t) + \boldsymbol{K}_x(t)\boldsymbol{x}_m(t) + \boldsymbol{K}_u(t)\boldsymbol{u}_m(t) \tag{17}$$

where $\boldsymbol{K}_e(t) \in \mathbb{R}^{3\times3}$ is the time-varying stabilizing control gain matrix, and $\boldsymbol{K}_x(t) \in \mathbb{R}^{3\times6}$ and $\boldsymbol{K}_u(t) \in \mathbb{R}^{3\times3}$ are time-varying feedforward control gains that contribute to achieving zero output tracking error. Practice shows that both $\boldsymbol{K}_x(t)$ and $\boldsymbol{K}_u(t)$ allow good tracking without requiring excessively large values of the stabilizing gain $\boldsymbol{K}_e(t)$. These control gains are generated by an adaptive algorithm that must maintain stability of the controlled system and bring the tracking error asymptotically toward zero. Specifically, the algorithm uses the measurable output feedback tracking error $\boldsymbol{e}_y$ to calculate the integral components of adaptive control gains so that they achieve a steepest descent minimization of the tracking errors, as follows:

$$\dot{\boldsymbol{K}}_{Ix}(t) = \boldsymbol{e}_y\boldsymbol{x}_m^T\Gamma_{Ix} \tag{18}$$

$$\dot{\boldsymbol{K}}_{Iu}(t) = \boldsymbol{e}_y\boldsymbol{u}_m^T\Gamma_{Iu} \tag{19}$$

where $\Gamma_{Iu} \in \mathbb{R}^{3\times3}$ and $\Gamma_{Ix} \in \mathbb{R}^{6\times6}$ are positive-definite diagonal matrices that define the adaptation rate of these control gains. Additionally, the integral component of the error adaptive control gain is introduced to maintain stability of the closed-loop system

$$\dot{\boldsymbol{K}}_{Ie}(t) = \boldsymbol{e}_y\boldsymbol{e}_y^T\Gamma_{Ie} \tag{20}$$

where $\Gamma_{Ie} \in \mathbb{R}^{3\times3}$ is the constant matrix defining the adaptation rate of $\boldsymbol{K}_{Ie}(t)$. Note that this integral gain corresponds to a monotonically increasing term that may potentially lead to instability under nonideal tracking situations, which may be due to measurement noise, for example. To mitigate this undesirable behavior, the adaptation mechanism will be slightly modified in Sec. VI such that the integral gains are obtained as a first-order filtering of the tracking errors.

Although only the integral adaptive control terms in Eqs. (18–20) are necessary to guarantee the stability of the direct adaptive control system [7], proportional adaptive control terms are added to increase the rate of convergence of the closed-loop system toward perfect tracking (as will be shown in Sec. V). Similar to the integral terms, these proportional adaptive control terms are obtained as

$$\boldsymbol{K}_{Pe}(t) = \boldsymbol{e}_y\boldsymbol{e}_y^T\Gamma_{Pe} \tag{21}$$

$$\boldsymbol{K}_{Px}(t) = \boldsymbol{e}_y\boldsymbol{x}_m^T\Gamma_{Px} \tag{22}$$

$$\boldsymbol{K}_{Pu}(t) = \boldsymbol{e}_y\boldsymbol{u}_m^T\Gamma_{Pu} \tag{23}$$

where $\Gamma_{Pe}, \Gamma_{Pu} \in \mathbb{R}^{3\times3}$, and $\Gamma_{Px} \in \mathbb{R}^{6\times6}$ are the constant coefficient matrices. Finally, the total adaptive gains are calculated by adding the integral terms to the proportional terms, as follows:

$$\boldsymbol{K}_e(t) = \boldsymbol{K}_{Pe}(t) + \boldsymbol{K}_{Ie}(t) \tag{24}$$

$$\boldsymbol{K}_x(t) = \boldsymbol{K}_{Px}(t) + \boldsymbol{K}_{Ix}(t) \tag{25}$$

$$\boldsymbol{K}_u(t) = \boldsymbol{K}_{Pu}(t) + \boldsymbol{K}_{Iu}(t) \tag{26}$$

The adaptive algorithm can then be rewritten concisely as

$$\boldsymbol{u} = \boldsymbol{K}(t)\boldsymbol{r} \tag{27}$$

where $\boldsymbol{K}(t) \in \mathbb{R}^{3\times12}$ and $\boldsymbol{r} \in \mathbb{R}^{12\times1}$ are respectively defined as

$$\boldsymbol{K}(t) = [\,\boldsymbol{K}_e(t) \quad \boldsymbol{K}_x(t) \quad \boldsymbol{K}_u(t)\,] = \boldsymbol{K}_P(t) + \boldsymbol{K}_I(t) \tag{28}$$

$$\boldsymbol{r} = [\,\boldsymbol{e}_y^T \quad \boldsymbol{x}_m^T \quad \boldsymbol{u}_m^T\,]^T \tag{29}$$

With this representation, $\boldsymbol{K}_P(t)$, $\boldsymbol{K}_I(t) \in \mathbb{R}^{3\times 12}$ are updated as follows:

$$\boldsymbol{K}_P(t) = \boldsymbol{e}_y \boldsymbol{r}^T \Gamma_P \tag{30}$$

$$\dot{\boldsymbol{K}}_I(t) = \boldsymbol{e}_y \boldsymbol{r}^T \Gamma_I \tag{31}$$

where Γ_P, $\Gamma_I \in \mathbb{R}^{12\times 12}$ are the resulting adaptation coefficient matrices for the combined gains $\boldsymbol{K}_p(t)$ and $\boldsymbol{K}_I(t)$, that is

$$\Gamma_P = \begin{bmatrix} \Gamma_{Pe} & & \\ & \Gamma_{Px} & \\ & & \Gamma_{Pu} \end{bmatrix}, \qquad \Gamma_I = \begin{bmatrix} \Gamma_{Ie} & & \\ & \Gamma_{Ix} & \\ & & \Gamma_{Iu} \end{bmatrix}$$

IV. Ideal Control and State Trajectory

As in the command generator tracker methodology [17], when the outputs of uncertain plant [Eq. (2)] tracks the output of the ideal model [Eq. (12)] perfectly, the plant is said to move along the bounded ideal state trajectory, denoted by $\boldsymbol{x}^* \in \mathbb{R}^6$. In other words, the ideal plant dynamics

$$\dot{\boldsymbol{x}}^* = \boldsymbol{A}\boldsymbol{x}^* + \boldsymbol{B}\boldsymbol{u}^*, \qquad \boldsymbol{y}^* = \boldsymbol{C}\boldsymbol{x}^* \tag{32}$$

moves along $\boldsymbol{x}^*$. Note that the ideal state $\boldsymbol{x}^*$ must be distinguished from the ideal model state $\boldsymbol{x}_m$ because the order of $\boldsymbol{x}^*$ always matches that of the actual plant $\boldsymbol{x}$, which may be (possibly) very large, whereas $\boldsymbol{x}_m$ can be of any order, even very low, just sufficiently large to generate the desired output signal $\boldsymbol{y}_m$. Furthermore, in Eq. (32), $\boldsymbol{u}^* \in \mathbb{R}^3$ denotes the ideal control law given by

$$\boldsymbol{u}^* = \tilde{\boldsymbol{K}}_e \boldsymbol{e}_y + \tilde{\boldsymbol{K}}_x \boldsymbol{x}_m + \tilde{\boldsymbol{K}}_u \boldsymbol{u}_m \tag{33}$$

Analogous to the adaptive control gains in the actual control law in Eq. (17), $\tilde{\boldsymbol{K}}_e \in \mathbb{R}^{3\times 3}$ denotes the constant ideal stabilizing gain matrix, whereas $\tilde{\boldsymbol{K}}_x \in \mathbb{R}^{3\times 6}$ and $\tilde{\boldsymbol{K}}_u \in \mathbb{R}^{3\times 3}$ are the constant ideal feedforward control gain matrices. Note that these ideal control gains are fictitious, not needed for implementation, and simply represent the constant gain values that result in perfect tracking, that is

$$\boldsymbol{e}_y = \boldsymbol{y}_m - \boldsymbol{y} = \boldsymbol{0}_3 \tag{34}$$

When this occurs, $\boldsymbol{u}^*$ reduces to

$$\boldsymbol{u}^* = \tilde{\boldsymbol{K}}_x \boldsymbol{x}_m + \tilde{\boldsymbol{K}}_u \boldsymbol{u}_m \tag{35}$$

Otherwise, there exists a state error, which is denoted by $\boldsymbol{e}_x \in \mathbb{R}^6$ and defined as

$$\boldsymbol{e}_x \triangleq \boldsymbol{x}^* - \boldsymbol{x} \tag{36}$$

In this case, the output tracking error $\boldsymbol{e}_y$ is no longer equal to zero and can be rewritten as

$$\boldsymbol{e}_y = \boldsymbol{C}\boldsymbol{x}^* - \boldsymbol{C}\boldsymbol{x} = \boldsymbol{C}\boldsymbol{e}_x \tag{37}$$

V. Stability

Before applying the adaptive control algorithm, it is necessary to guarantee closed-loop stability to show that the errors asymptotically converge to zero and that the control gains are bounded. To this end, the differential equation of the state error is obtained by differentiating with respect to time Eq. (36), which results in

$$\dot{\boldsymbol{e}}_x = (\boldsymbol{A} - \boldsymbol{B}\tilde{\boldsymbol{K}}_e \boldsymbol{C})\boldsymbol{e}_x - \boldsymbol{B}(\boldsymbol{K}_I(t) - \tilde{\boldsymbol{K}})\boldsymbol{r} - \boldsymbol{B}\boldsymbol{K}_P(t)\boldsymbol{r} \tag{38}$$

where $\tilde{\boldsymbol{K}} \in \mathbb{R}^{3\times 12}$ is

$$\tilde{\boldsymbol{K}} = [\,\tilde{\boldsymbol{K}}_e \quad \tilde{\boldsymbol{K}}_x \quad \tilde{\boldsymbol{K}}_u\,] \tag{39}$$

Theorem 2: The application of the passivity-based adaptive control law in Eqs. (27, 30, 31) to the relative dynamics represented as an LTI state-space system with a scaled-position-and-velocity output matrix in Eqs. (2) and 6) ensures that all adaptive control gains are bounded under closed-loop operation and results in asymptotic convergence of the state and output tracking errors, in the sense that

$$\|\boldsymbol{e}_y\| \to 0 \quad \text{and} \quad \|\boldsymbol{e}_x\| \to 0 \quad \text{as} \quad t \to \infty$$

where $\|\cdot\|$ denotes the standard Euclidean norm of a vector.

Proof: Let define a continuously differentiable positive-definite quadratic Lyapunov function of the form

$$V(t) = \boldsymbol{e}_x^T \boldsymbol{P} \boldsymbol{e}_x + \mathrm{tr}[(\boldsymbol{K}_I(t) - \tilde{\boldsymbol{K}})\Gamma_I^{-1}(\boldsymbol{K}_I(t) - \tilde{\boldsymbol{K}})^T] \tag{40}$$

Taking the time derivative of Eq. (40) and substituting $\boldsymbol{K}_P(t)$ and $\dot{\boldsymbol{K}}_I(t)$ with Eqs. (30) and (31), respectively, and $\boldsymbol{e}_y$ and $\dot{\boldsymbol{e}}_x$ with Eqs. (37) and (38), respectively, and making use of Theorem 1, i.e., using the ASP relations given by Eqs. (10) and (11), results in the following time-derivative of the Lyapunov function:

$$\dot{V}(t) = -\boldsymbol{e}_x^T \boldsymbol{Q} \boldsymbol{e}_x - 2\boldsymbol{e}_x^T \boldsymbol{C}^T \boldsymbol{C} \boldsymbol{e}_x \boldsymbol{r}^T \Gamma_P \boldsymbol{r} \tag{41}$$

The Lyapunov derivative in Eq. (41) only includes the state error $\boldsymbol{e}_x$ and is therefore negative-definite in $\boldsymbol{e}_x$ and negative-semidefinite in the state-gain space $[\boldsymbol{e}_x, \boldsymbol{K}_I(t)]$. Thus, the stability of the adaptive system with respect to boundedness is guaranteed by the Lyapunov direct method [8] as well as all state and output errors, and adaptive control gains are bounded.

Furthermore, asymptotic stability of the tracking errors is demonstrated by invoking LaSalle's invariance principle for nonautonomous systems [7,9–11], which states that, for a negative semidefinite Lyapunov derivative of the form of Eq. (41), all system trajectories are contained within the domain $\Omega_0 = \{[\boldsymbol{e}_x, \boldsymbol{K}_I(t)] | V([\boldsymbol{e}_x, \boldsymbol{K}_I(t)], t) \le V([\boldsymbol{e}_{x_0}, \boldsymbol{K}_{I_0}(t)], 0)\}$, where the subscript $\{\}_0$ denotes the initial conditions, and the entire state space $[\boldsymbol{e}_x, \boldsymbol{K}_I(t)]$ ultimately reaches the domain $\Omega_f = \Omega_0 \cap \Omega$, where Ω denotes the domain defined by the Lyapunov derivative identical to zero. In other words, the state space $[\boldsymbol{e}_x, \boldsymbol{K}_I(t)]$ ultimately reaches the domain defined by $\dot{V}([\boldsymbol{e}_x, \boldsymbol{K}_I(t)], t) \equiv 0$ [12]. Because $\dot{V}([\boldsymbol{e}_x, \boldsymbol{K}_I(t)], t)$ is negative-definite in $\boldsymbol{e}_x$, the system ends with $\boldsymbol{e}_x \equiv 0$. Finally, because $\boldsymbol{e}_x \equiv 0$ implies $\boldsymbol{e}_x = \boldsymbol{e}_y = 0$, asymptotic stability of the state and output tracking errors is guaranteed. □

VI. Tracking Under Nonideal Conditions

It is well known that in the original form of the adaptive control law, the integral time-varying control gain $\boldsymbol{K}_I(t)$ could exhibit undesirable divergence behavior under nonideal conditions. A possible solution to this problem is the σ modification pioneered by the work of Narendra et al. [18], which studied the effects of perturbations on stability of conventional model reference adaptive control (MRAC) systems and widely popularized in the work of Ioannou and Kokotovic [19,20], Barkana and Kaufman [21,22], and Narendra and Annaswamy [23]. The first σ modification for SAC (or implicit MRAC) was proposed by Fradkov [24]. The simplest form of σ modification is adopted in this Note, without any switching rules or other modifications proposed in the literature. Specifically, this modification consists of adding additional terms in the integral gain adaptation mechanisms, widely referred to as forgetting terms or forgetting factors. With this adjustment, the time-varying integral control gains are obtained as

$$\dot{\boldsymbol{K}}_{I_e}(t) = \boldsymbol{e}_y \boldsymbol{e}_y^T \Gamma_{I_e} - \sigma_e \boldsymbol{K}_{I_e}(t) \tag{42}$$

$$\dot{\boldsymbol{K}}_{I_x}(t) = \boldsymbol{e}_y \boldsymbol{x}_m^T \Gamma_{I_x} - \sigma_x \boldsymbol{K}_{I_x}(t) \tag{43}$$

$$\dot{\boldsymbol{K}}_{I_u}(t) = \boldsymbol{e}_y \boldsymbol{u}_m^T \Gamma_{I_u} - \sigma_u \boldsymbol{K}_{I_u}(t) \tag{44}$$

and similarly,

$$\dot{\boldsymbol{K}}_I(t) = \boldsymbol{e}_y \boldsymbol{r}^T \Gamma_I - \sigma \boldsymbol{K}_I(t) \tag{45}$$

where

$$\sigma = \begin{bmatrix} \sigma_e & & \\ & \sigma_x & \\ & & \sigma_u \end{bmatrix} \in \mathbb{R}^{12\times 12}$$

where $\sigma_e \in \mathbb{R}^{3\times 3}$, $\sigma_x \in \mathbb{R}^{3\times 6}$, $\sigma_u \in \mathbb{R}^{3\times 3}$, and $\sigma_I \in \mathbb{R}^{12\times 12}$ denote the forgetting term matrices. With this modification to the adaptive algorithm, the Lyapunov derivative function becomes

$$\dot{V}(t) = -\boldsymbol{e}_x^T \boldsymbol{Q} \boldsymbol{e}_x - 2\boldsymbol{e}_x^T \boldsymbol{C}^T \boldsymbol{C} \boldsymbol{e}_x \boldsymbol{r}^T \Gamma_P \boldsymbol{r} - 2\mathrm{tr}[\sigma_I \boldsymbol{K}_I(t) \Gamma_I^{-1} (\boldsymbol{K}_I(t) - \tilde{\boldsymbol{K}})^T] \tag{46}$$

Thus, according to the Lyapunov direct method and LaSalle's invariance principle, the application of the algorithm with the forgetting terms results in bounded error tracking. It is notable that, although it affects the proof of stability, using the passivity-based adaptive control law with this adjustment is preferred in most practical applications where measurements are corrupted by noise. Indeed, without the forgetting terms the integral adaptive gains can increase for as long as there is a tracking error. When the integral gains reach certain values, they have a stabilizing effect on the system, and the tracking error begins to decrease. However, if the tracking error does not reach zero for some reason, the integral gains will continue to increase and eventually diverge. On the other hand, with the forgetting terms, the integral gains increase as required (e.g., due to large tracking errors) and decrease when large gains are no longer necessary. In fact, with this modification, the integral gains are obtained as a first-order filtering of the tracking errors and cannot diverge unless the tracking errors diverge.

It is important to note that, as the adaptation progresses and the adaptive gains stabilize the system, the tracking error (and thus the adaptive gains) start decreasing. If the gains go below minimal stabilizing values, a sudden burst of tracking errors may occur. However, thanks to this burst, the tracking errors suddenly increase, which drives the gains to also suddenly increase and the tracking errors to start decreasing, and so on. This is the error-bursting phenomenon inherent to the σ-modified adaptive controller. Obviously, one way to prevent this is to impose lower bounds on the gains. Yet recent results [25] demonstrate that a more effective solution consists in applying a forgetting term only on $\dot{\boldsymbol{K}}_{I_e}(t)$ because anyway the gains related to $\boldsymbol{x}_m$ and $\boldsymbol{u}_m$ do not necessarily need a forgetting term since there is no correlation between these two signals and measurement noise. Furthermore, this may lead to further improvements of tracking performance. Nevertheless, because bursting did not occur in this work (both in simulation and experiment), the forgetting terms were kept on all three adaptive gains, according to Eqs. (42–44).

VII. Simulation Example

Numerical simulations in MATLAB/Simulink were performed to assess the effectiveness of the proposed control approach against a standard nonadaptive proportional–derivative controller. Uncertainties in its dynamics model and parameter make the plant challenging to be controlled by conventional control methodologies. The nominal design conditions are defined by the double-integrator model with no external perturbations (as suggested by Fehse [4]) and a free-flyer servicer robot with mass $m = 4.3$ kg. In other words, both controllers were tuned in numerical simulations when applied to the unperturbed double-integrator dynamics model. The control parameters were chosen as

$$\Gamma_{Pe} = 5e-4\boldsymbol{I}_{3\times 3}, \qquad \Gamma_{Px} = 1e-4\boldsymbol{I}_{6\times 6},$$
$$\Gamma_{Pu} = 1e-4\boldsymbol{I}_{3\times 3} \quad \Gamma_{Ie} = 2\boldsymbol{I}_{3\times 3}, \Gamma_{Ix} = \boldsymbol{I}_{6\times 6}, \qquad \Gamma_{Iu} = \boldsymbol{I}_{3\times 3}$$

and

$$\sigma = 0.1\boldsymbol{I}_{12\times 12}$$

These control parameters were selected to achieve a satisfactory response under nominal design conditions. Furthermore, it is important to note that the Γ parameters only define the adaptation rates of the control gains, not the control gains themselves. As such, they could have been selected significantly larger to enable the control gains to vary rapidly, to yield tracking performance with faster transient responses. Smaller values for the adaptation rates, resulting in lower rates of change in the adaptive gains, were herein selected because they exhibited satisfactory response. The adaptation algorithm was initialized with $\boldsymbol{K}_{Ie} = \boldsymbol{K}_{Iu} = 0_{3\times 3}$ and $\boldsymbol{K}_{Ix} = 0_{3\times 6}$, and the integral structure of the adaptive gains was computed with a fixed-time-step fifth-order Runge–Kutta integration scheme. The ideal model was designed to incorporate the desired input–output behavior described by $\zeta = 0.9$ and $\omega_n = 0.13$ rad/s. The ratio of position to velocity output, α, was set to 0.1 for both the plant and the reference model. The specific values of ζ and ω_n were determined such that the ideal model provides a settling time and maximum overshoot similar to that of the following PD state-feedback controller:

$$\boldsymbol{u} = \boldsymbol{K}_P \begin{bmatrix} x_d - x \\ y_d - y \\ z_d - z \end{bmatrix} + \boldsymbol{K}_D \begin{bmatrix} \dot{x}_d - \dot{x} \\ \dot{y}_d - \dot{y} \\ \dot{z}_d - \dot{z} \end{bmatrix} \tag{47}$$

where $\boldsymbol{K}_P$, $\boldsymbol{K}_D \in \mathbb{R}^{3\times 3}$ are constant control gain matrices tuned previously by Nolet [26] to give optimal tracking performance for this specific problem, under nominal conditions (i.e., for the unperturbed double-integrator model with $m = 4.3$ kg):

$$\boldsymbol{K}_P = 0.172\boldsymbol{I}_{3\times 3}, \qquad \boldsymbol{K}_D = 1.720\boldsymbol{I}_{3\times 3}$$

Similar to de Queiroz et al. [6], the desired relative trajectory was selected as

$$[\,x_d(t) \quad y_d(t) \quad z_d(t)\,]^T = [\,0 \quad 100\cos(\omega t) \quad 100\sin(\omega t)\,]^T \text{ m}$$

with $\omega = 2\pi/300$ rad/s. The relative position and velocity were initialized as

$$[\,x_0 \quad y_0 \quad z_0\,]^T = [\,0 \quad -0.2 \quad 0\,]^T \text{ m}$$
$$[\,\dot{x}_0 \quad \dot{y}_0 \quad \dot{z}_0\,]^T = [\,0 \quad 0 \quad 0\,]^T \text{ m/s}$$

The desired trajectory and initial conditions represent a servicer robot that is initially at rest with respect to the target spacecraft and is then commanded to perform a fly-around maneuver around the target in a circular trajectory with radius of 100 m in the along-track/cross-track (y-z) plane with a constant angular velocity ω. Note that the selection of this desired relative trajectory does not take into account any fuel-consumption considerations. Nevertheless, it illustrates the capability of the controllers to track demanding trajectories that may occur during reconfiguration maneuvers.

Although one of the practical purposes of the adaptive controller is to achieve robust performance under large mass variations caused by the harvesting of unknown components from a target spacecraft, the

strongest demonstration consists of varying the mass of the servicer robot. To this end, numerical simulations with a larger mass were performed to assess the robustness of the proposed controller to parametric uncertainties in the plant. Specifically, the uncertain mass is defined by $m = 9.7$ kg, which represents a 225% increase of the servicer robot mass. In the context of DARPA's Phoenix Program, the uncertain mass scenario represents the case where the servicer robot has retrieved a component of unknown mass from a decommissioned target spacecraft. In addition, robustness to neglected dynamics effects is evaluated by applying the controllers tuned with the double-integrator model to the CW model. To simulate the CW model, the orbital mean motion was calculated as $n = \sqrt{\mu/a^3}$, with $a \in \mathbb{R}$ denoting the semimajor axis of the target spacecraft orbit (7200 km) and $\mu \in \mathbb{R}$ denoting the gravitational parameter of the Earth ($398,600\ \text{km}^3/\text{s}^2$). Finally, robustness to unknown external perturbations is assessed by considering the following perturbation forces (unknown to the controller) to the plant:

$$\boldsymbol{u}_{\text{per}}(t) = [\,1 + \sin(0.1t) \quad 1 + \sin(0.1t) \quad 1 + \sin(0.1t)\,]^T \text{ N}$$

Results obtained by using the control laws defined previously (i.e., with control parameters tuned for the unperturbed double-integrator model with $m = 4.3$ kg) are provided in Fig. 1. As expected, and as shown in this figure, both control approaches yield satisfactory relative motion tracking under nominal conditions. Additionally, there is no apparent difference between the double-integrator and the CW responses, which indicates that neglecting the orbital dynamics effects introduced in the CW model does not affect the controller tracking performance, at least when the maximum separation is on the order of a few tens of meters and when the time scale is much faster than the orbital period. Indeed, as discussed earlier, under these conditions, the coupling terms in the CW model are much smaller than the remaining double-integrator terms in the CW equations. In other words, the orbital dynamics uncertainties inherent to the simple double-integrator model are not significant enough to deteriorate the tracking performance of both controllers. However, in the presence of dynamics uncertainty and large unknown external perturbation forces, the PD controller yields larger trajectory overshoots and sustained oscillations that fail to converge to the desired relative trajectory, whereas the adaptive controller provides similar responses, regardless of the presence of unknown external perturbation forces, as shown in Fig. 2. This demonstrates the improved robustness to parametric uncertainties and external perturbations achieved with the adaptive strategy.

The improved behavior associated with the direct adaptive control strategy is possible because the time-varying control gains, shown in Figs. 3 and 4 ($\boldsymbol{K}_e(t)$ only, for conciseness), are adapting to maintain minimal tracking errors under different adverse conditions.

VIII. Experimental Results

To demonstrate the applicability of the passivity-based adaptive control law to realistic free-flyer space robots with limited computational resources, an experiment was performed with the Synchronized Position Hold Engage Reorient Experimental Satellites (SPHERES) air bearing flat floor facility at the Massachusetts Institute of Technology Space Systems Laboratory. SPHERES is an experimental testbed consisting of a group of small

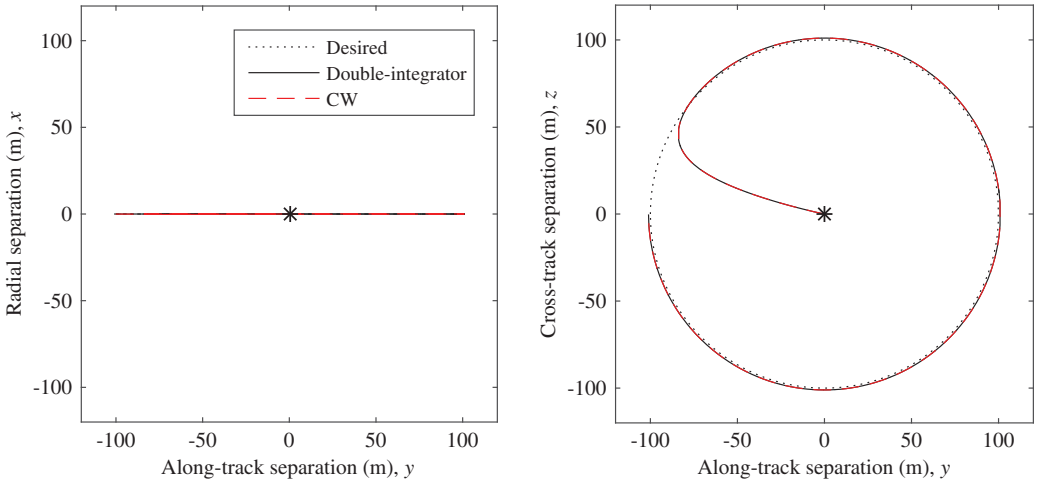

a) PD controller

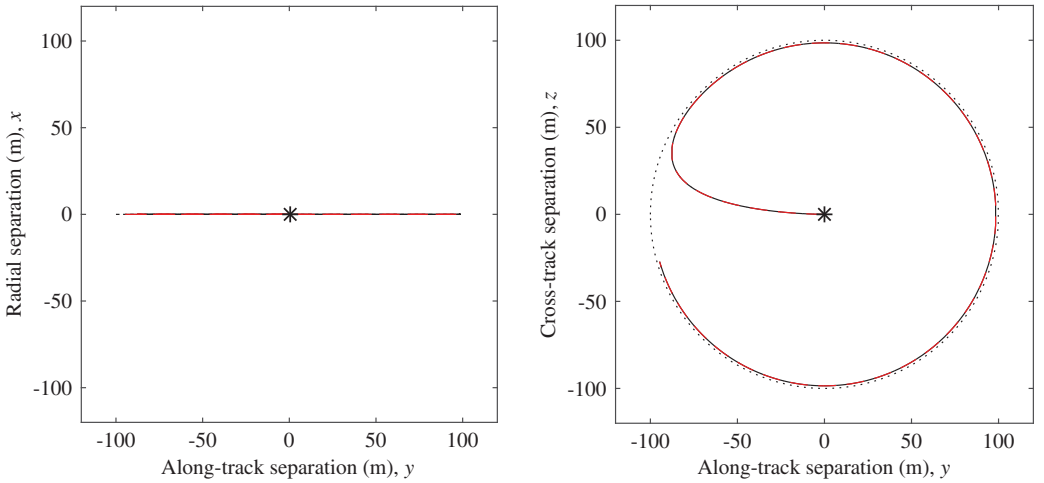

b) Adaptive controller

Fig. 1 Unperturbed double-integrator and CW relative motion with $m = 4.3$ kg.

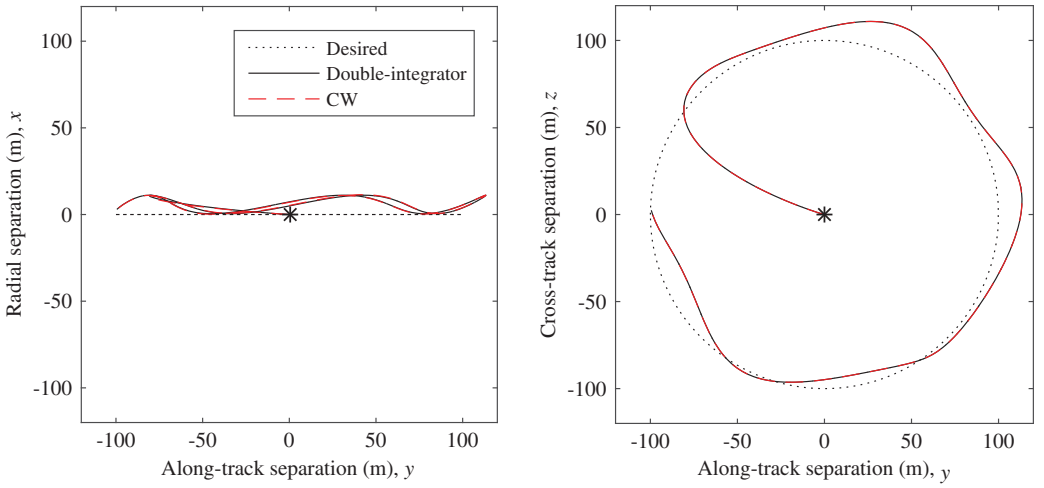

a) PD controller

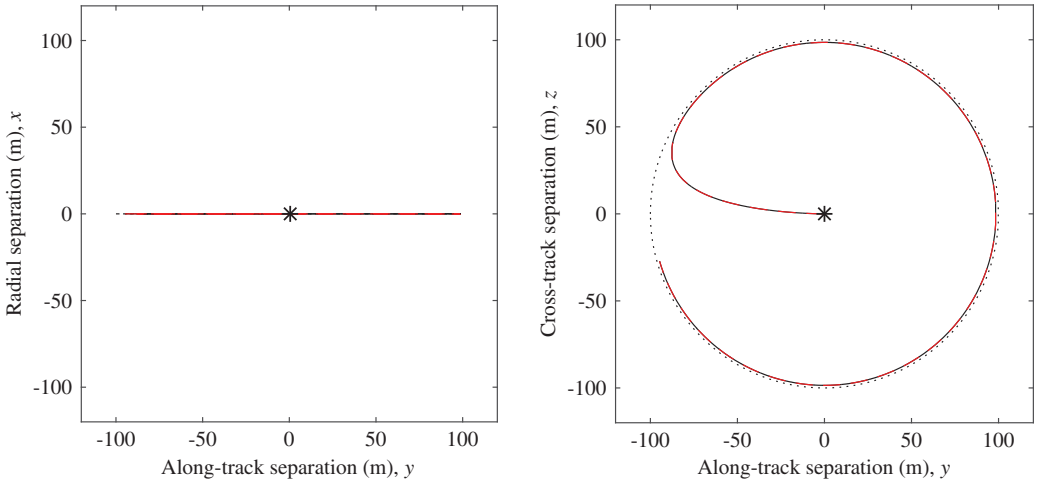

b) Adaptive controller

Fig. 2 Perturbed double-integrator and CW relative motion with $m = 9.7$ kg.

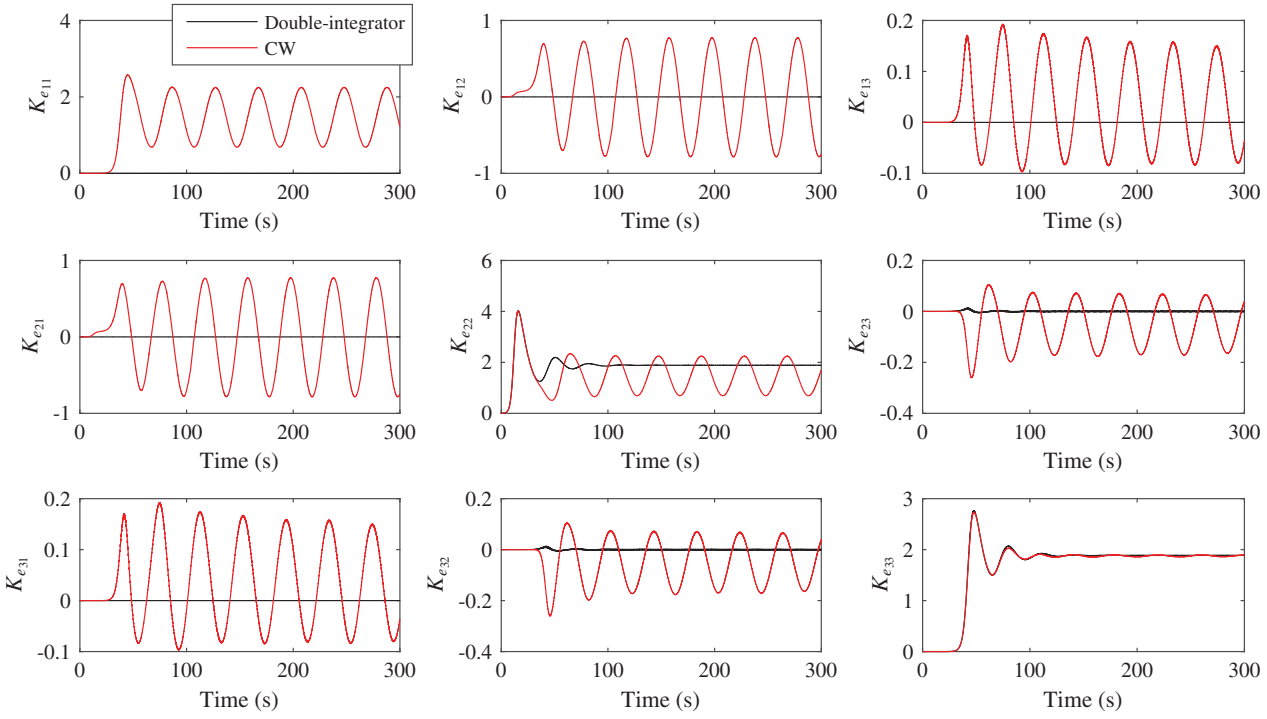

Fig. 3 Adaptation history of output error control gain $K_e(t)$ with $m = 4.3$ kg.

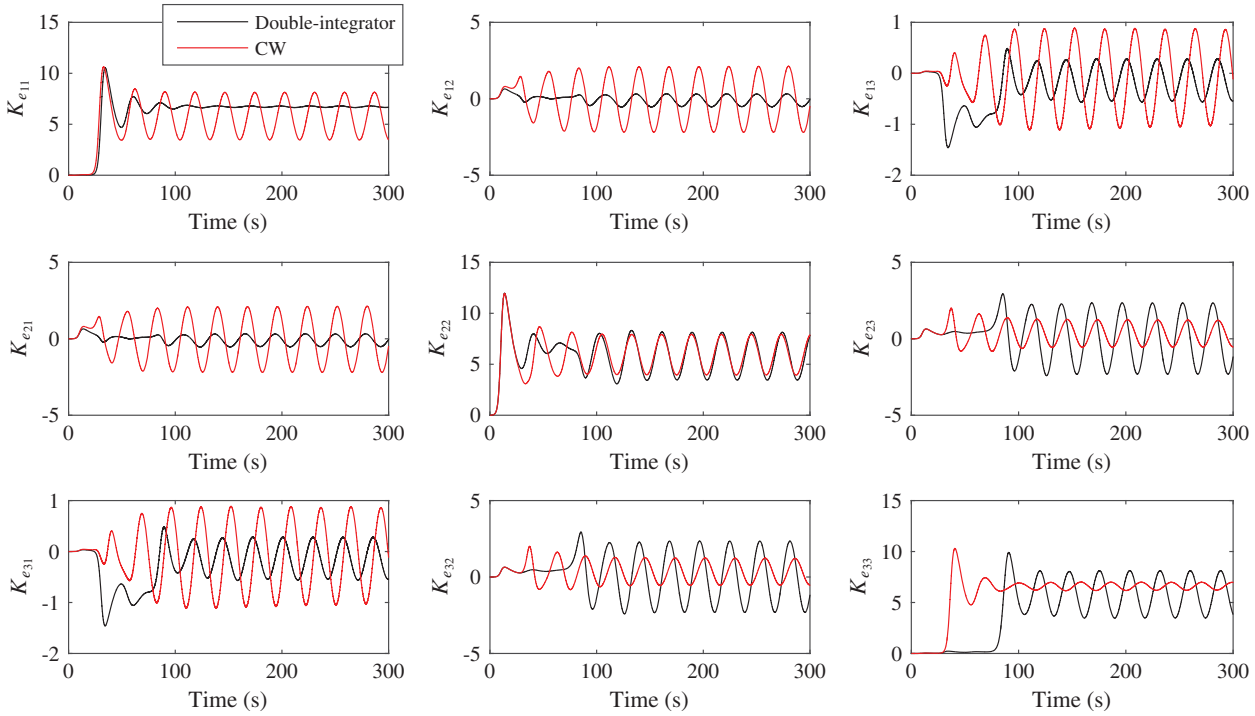

Fig. 4 Adaptation history of output error control gain $K_e(t)$ with $m = 9.7$ kg and external perturbations.

autonomous platforms with the basic functionalities of realistic nanosatellites [27]. Propulsion is provided by CO_2 thrusters, and their inertial positioning systems are based on an extended Kalman filter (EKF) that estimates states variables based on measurements from an inertial measurement unit (IMU) at 20 Hz and from the time of flight of ultrasound pulses generated at 5 Hz by beacons located at known positions within the test area [28]. Each robotic spacecraft platform is programmed in C code via the Texas Instruments Code Composer Studio's Integrated Development Environment, which provides the interfaces to the C6701 digital signal processing (DSP) unit aboard the robot platforms. The interfaces include access to real-time threads for estimation and control. However, the DSP has limited processing capabilities because it operates at 167 MHz and has 16 MB of RAM and 256 kB of available flash memory. Figure 5 shows the robotic spacecraft platforms that were used for the experiment.

The maneuver for the experiment is relatively simple. Both vehicles are initially at rest, then the servicer robot is commanded to undock from the target spacecraft and move 1 m along the x axis. This particular maneuver was selected because it represents a classical step input from which the transient characteristics of the experimental closed-loop system can easily be determined. For the experiment, only the 9.7 kg perturbed double-integrator conditions could be tested because both SPHERES had to be installed on air carriages to allow them to float on the epoxy flat floor, which increased their nominal mass from 4.3 to 9.7 kg. Similar to the simulation example discussed in the previous section, the control parameters were selected to provide satisfactory performance under nominal conditions using the SPHERES simulation facility. This allowed the robustness of the adaptive control law to large mass uncertainty and unknown perturbations to be validated. The SPHERES simulation facility is a C/C++ high-fidelity simulation environment that models the actual platform hardware components, including actuators, sensors, multiple thread computing, limited available computing power, time delays, and noise.

Figure 6 shows the experimental results of the 133 s test for the PD controller left graph and the adaptive controller right graph. During the first 10 s, both vehicles are at rest in a docking configuration,

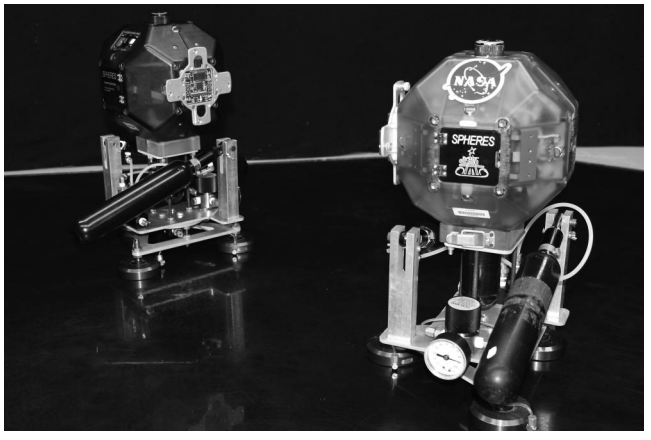

Fig. 5 Two SPHERES platforms operating in close proximity.

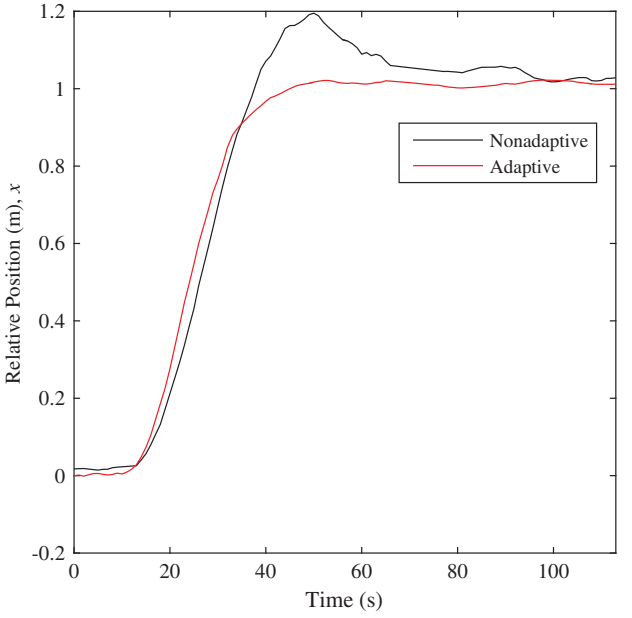

Fig. 6 Perturbed double-integrator experimental results with $m = 9.7$ kg.

during which time the EKF converges to a solution using the IMU and ultrasonic beacon system. At 10 s into the experiment, the servicer robot platform starts to maneuver through autonomous control by opening the solenoid valves regulating the airflow to its air nozzles. As shown in Fig. 6, better tracking performance under off-nominal conditions is achieved by the adaptive control law, compared to the PD controller. This is illustrated by the maximum trajectory overshoot at 45 s of 0.20 m for the PD control law and 0.02 m for the passivity-based adaptive control law. This increase in performance is attributable to the time-varying control gains shown in Fig. 7, which adapted to the current tracking situation by reaching the most effective values at any given time to maintain the trajectory tracking performance under adverse/unknown conditions. As expected, and as demonstrated by the results, the constant control gain strategy does not provide a satisfactory response because the gains were tuned for the nominal case. Indeed, to achieve good results when the mass of the servicer robot is significantly increased, the gains must be tuned such that larger control input forces are applied. This is shown in Fig. 8, where the resulting control input force for the PD controller reaches lower values compared to that obtained with the adaptive controller. In turn, the low PD control input force does not prove to be adequate to control the relative position under off-nominal conditions.

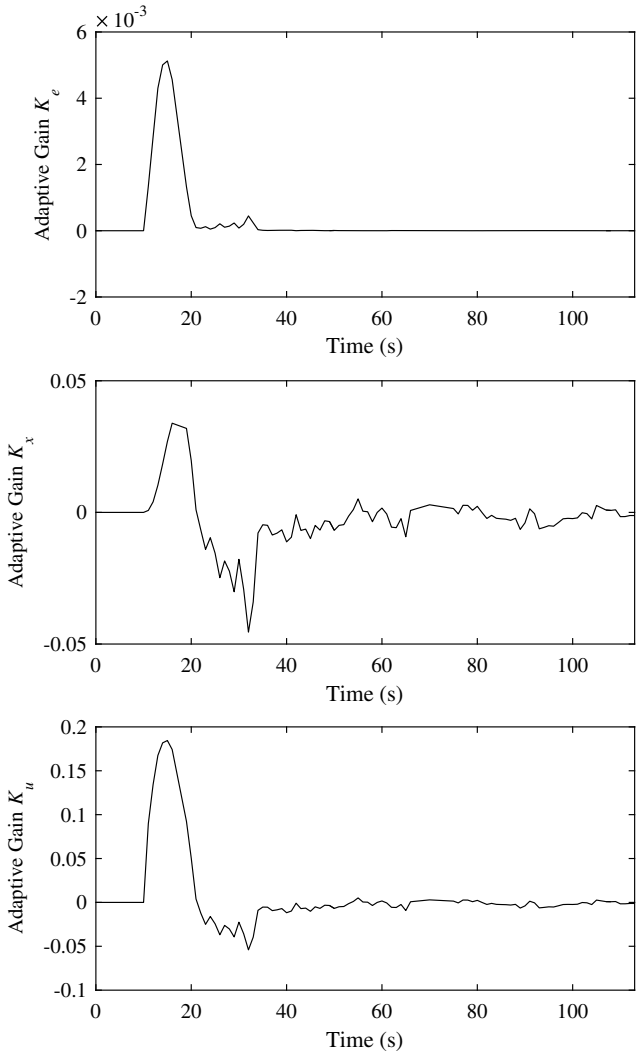

Fig. 7 Experimental control gains adaptation history.

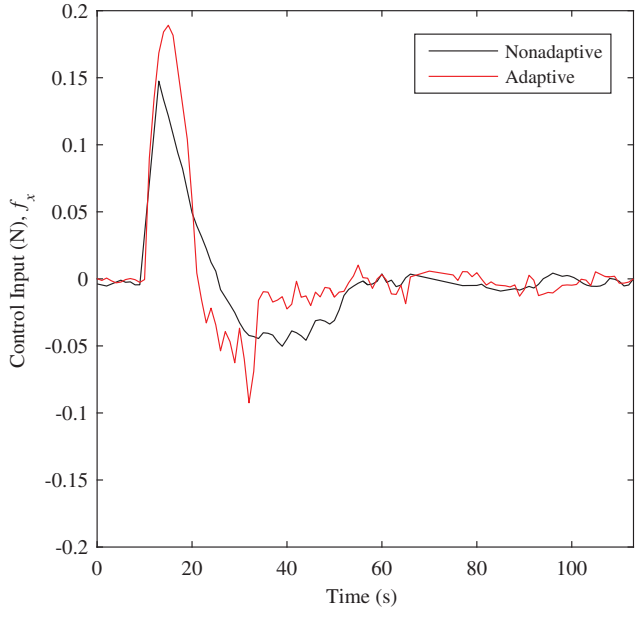

Fig. 8 Experimental control input force f_x.

IX. Conclusions

This Note addressed the problem of adaptive trajectory tracking control for free-flyer robotic spacecraft in close-proximity operations under dynamics uncertainty and unknown external perturbations. Specifically, a passivity-based output feedback adaptive control law was proposed, which was shown to satisfy the almost strictly passive (ASP) conditions that were required for stability demonstration purposes, through the Lyapunov direct method and LaSalle's invariance principle arguments. In numerical simulations, the adaptive control strategy improved both tracking results and robustness under off-nominal conditions, compared to a proportional–derivative (PD) controller. The robustness and simplicity of this adaptive algorithm makes this controller well suited for real-time implementation onboard a small free-flyer robot with limited computing power, as demonstrated by an experiment performed with the Synchronized Position Hold Engage Reorient Experimental Satellites (SPHERES) facility at the Massachusetts Institute of Technology's Space Systems Laboratory.

Acknowledgments

Part of this work was supported by the Natural Sciences and Engineering Research Council of Canada under the Postdoctorate Fellowship Award PDF-438572-2013 while Steve Ulrich was Postdoctoral Associate at the Massachusetts Institute of Technology. The authors also thank the anonymous reviewers and Associate Editor for their useful comments that helped to significantly improve this Note.

References

[1] Kawano, I., Mokuno, M., Kasai, T., and Suzuki, T., "Result of Autonomous Rendezvous Docking Experiment of Engineering Test Satellite-VII," *Journal of Spacecraft and Rockets*, Vol. 38, No. 1, 2001, pp. 105–111. doi:10.2514/2.3661

[2] Weismuller, T., and Leinz, M., "GN&C Technology Demonstrated by the Orbital Express Autonomous Rendezvous and Capture Sensor System," *Proceedings of the 29th Annual AAS Guidance and Control Conference*, American Astronomical Soc. Paper 06-016, Washington, D.C., 2006.

[3] Clohessy, W. H., and Wiltshire, R. S., "Terminal Guidance System for Satellite Rendezvous," *Journal of the Aerospace Sciences*, Vol. 27, No. 9, 1960, pp. 653–658. doi:10.2514/8.8704

[4] Fehse, W., *Automated Rendezvous and Docking of Spacecraft*, Cambridge Univ. Press, Cambridge, England, U.K., 2003, pp. 192–193.

[5] Egardt, B., *Stability of Adaptive Controllers*, Springler–Verlag, Berlin, 1979, pp. 1–8.

[6] de Queiroz, M. S., Vikram, K., and Qiguo, Y., "Adaptive Nonlinear Control of Multiple Spacecraft Formation Flying," *Journal of Guidance,*

Control, and Dynamics, Vol. 23, No. 3, 2000, pp. 385–390. doi:10.2514/2.4549

[7] Barkana, I., "Simple Adaptive Control—A Stable Direct Model Reference Adaptive Control Methodology—Brief Survey," *International Journal of Adaptive Control and Signal Processing*, Vol. 28, Nos. 7–8, 2014, pp. 583–594. doi:10.1002/acs.2411

[8] Slotine, J. J. E., and Li, W., *Applied Nonlinear Control*, Prentice–Hall, Englewood Cliffs, NJ, 1991, pp. 123–126.

[9] LaSalle, J. P., "Stability of Nonautonomous Systems," *Nonlinear Analysis: Theory, Methods & Applications*, Vol. 1, No. 1, 1976, pp. 83–90. doi:10.1016/0362-546X(76)90011-0

[10] Kaufman, H., Barkana, I., and Sobel, K., *Direct Adaptive Control Algorithms: Theory and Applications*, 2nd ed., Communications and Control Engineering Series, Springer, New York, 1997, pp. 39–45.

[11] LaSalle, J. P., *The Stability of Dynamical Systems*, 2nd ed., Soc. for Industrial and Applied Mathematics, New York, 1976, p. 43.

[12] Barkana, I., "The New Theorem of Stability—Direct Extension of Lyapunov Theorem," *Mathematics in Engineering, Science and Aerospace*, Vol. 6, No. 3, 2015, pp. 519–535.

[13] Ortega, R., and Spong, M. W., "Adaptive Motion Control of Rigid Robots: A Tutorial," *Automatica*, Vol. 25, No. 6, 1989, pp. 877–888. doi:10.1016/0005-1098(89)90054-X

[14] Saulnier, K., Perez, D., Huang, R. C., Gallardo, D., Tilton, G., and Bevilacqua, R., "A Six-Degree-of-Freedom Hardware-in-the-Loop Simulator for Small Spacecraft," *Acta Astronautica*, Vol. 105, No. 2, 2014, pp. 444–462. doi:10.1016/j.actaastro.2014.10.027

[15] Paluszek, M., and Thomas, S., "Generalized 3D Spacecraft Proximity Path Planning Using A*," *AIAA Infotech@Aerospace*, AIAA Paper 2005-7043, Sept. 2005.

[16] Barkana, I., "Comments on Design of Strictly Positive Real Systems Using Constant Output Feedback," *IEEE Transactions on Automatic Control*, Vol. 49, No. 11, 2004, pp. 2091–2093. doi:10.1109/TAC.2004.837565

[17] O'Brien, M., and Broussard, R., "Feedforward Control to Track the Output of a Forced Model," *IEEE Transactions on Automatic Control*, Vol. 23, No. 4, 1980, pp. 851–853. doi:10.1109/TAC.1980.1102409

[18] Narendra, K. S., Tripathi, S. S., Luders, G., and Kudva, P., "Adaptive Control Using Lyapunov's Direct Method," Yale Univ. TR CT-43, New Haven, CT, 1971.

[19] Ioannou, P. A., and Kokotovic, P., *Adaptive Systems with Reduced Models*, Springer–Verlag, New York, 1983, pp. 81–90.

[20] Ioannou, P. A., and Kokotovic, P., "Instability Analysis and Improvement of Robustness of Adaptive Control," *Automatica*, Vol. 20, No. 5, 1984, pp. 583–594. doi:10.1016/0005-1098(84)90009-8

[21] Barkana, I., and Kaufman, H., "Direct Adaptive Control with Bounded Tracking Errors," *Proceedings of the 22nd IEEE Conference on Decision and Control*, IEEE Publ., Piscataway, NJ, 1983, pp. 221–222.

[22] Barkana, I., and Kaufman, H., "Robust Simplified Adaptive Control for a Class of Multivariable Systems," *Proceedings of the 24th IEEE Conference on Decision and Control*, IEEE Publ., Piscataway, NJ, 1985, pp. 141–146.

[23] Narendra, K. S., and Annaswamy, A. M., *Stable Adaptive Systems*, Springer–Verlag, Englewood Cliffs, NJ, 1989, pp. 291–358.

[24] Fradkov, A. L., "Quadratic Lyapunov Function in the Adaptive Stabilization Problem of a Linear Dynamic Plant," *Siberian Mathematical Journal*, Vol. 17, No. 2, 1976, pp. 341–348. doi:10.1007/BF00967581

[25] Barkana, I., "Robustness and Perfect Tracking in Simple Adaptive Control," *International Journal of Adaptive Control and Signal Processing* (to be published). doi:10.1002/acs.2573

[26] Nolet, S., "Development of a Guidance, Navigation and Control Architecture and Validation Process Enabling Autonomous Docking to a Tumbling Satellite," Ph.D. Thesis, Massachusetts Inst. of Technology, Dept. of Aeronautics and Astronautics, Cambridge, MA, 2007.

[27] Mohan, S., Saenz-Otero, A., Nolet, S., Miller, D., and Sell, S., "SPHERES Flight Operations Testing and Execution," *Acta Astronautica*, Vol. 65, No. 7, 2009, pp. 1121–1132. doi:10.1016/j.actaastro.2009.03.039

[28] Nolet, S., "The SPHERES Navigation System: From Early Development to On-Orbit Testing," *AIAA Guidance, Navigation, and Control Conference and Exhibit*, AIAA Paper 2007-6354, Aug. 2007.